

## Coarse-grained molecular dynamics simulations of shear-induced instabilities of lipid bilayer membranes in water

Itsuo Hanasaki,<sup>1,\*</sup> Jens H. Walther,<sup>2,3,†</sup> Satoyuki Kawano,<sup>1,‡</sup> and Petros Koumoutsakos<sup>2,§</sup>

<sup>1</sup>*Department of Mechanical Science and Bioengineering, Graduate School of Engineering Science, Osaka University, Machikaneyama-cho 1-3, Toyonaka, Osaka 560-8531, Japan*

<sup>2</sup>*Chair of Computational Science, ETH Zürich, Universitätsstrasse 6, CH-8092 Zürich, Switzerland*

<sup>3</sup>*Department of Mechanical Engineering, Technical University of Denmark, DK-2800 Lyngby, Denmark*

(Received 14 January 2010; revised manuscript received 10 September 2010; published 9 November 2010)

We study shear-induced instabilities of lipid bilayers immersed in water using coarse-grained molecular dynamics simulations. The shear imposed by the flow of the water induces initially microscopic structural changes of the membrane, starting with tilting of the molecules in the direction of the shear. The tilting propagates in the spanwise direction when the shear rate exceeds a critical value and the membrane undergoes a bucklinglike deformation in the direction perpendicular to the shear. The bucklinglike undulation continues until a localized Kelvin-Helmholtz-like instability leads to membrane rupture. We study the different modes of membrane undulation using membranes of different geometries and quantify the relative importance of the bucklinglike bending and the Kelvin-Helmholtz-like instability of the membrane.

DOI: [10.1103/PhysRevE.82.051602](https://doi.org/10.1103/PhysRevE.82.051602)

PACS number(s): 68.08.-p

### I. INTRODUCTION

The composition, structure, and deformation of cell membranes are critical for the functioning of cells interacting with flowing liquids either in natural settings such as blood flow or in engineering devices such as microfluidic cell sorters [1]. The response of endothelial cells to shear is important for the development of aneurysms [2], the progression of tumor-induced angiogenesis [3], and tissue morphoregulation [4]. In microfluidic devices hemolysis and cell rupture are known to depend on the amount of shear that can be sustained by the cell membrane [5]. Flow shear enhances the molecular permeability of cell membranes under *in vitro* conditions [6] and has also been used for cell separation and filtration [6]. The efficiency of these processes increases with the level of the shear. However, above a certain shear threshold value the cell membrane may be damaged. This is a result of excessive membrane deformations that are imparted to the membrane by stress-induced membrane instabilities. The material properties of the membrane may result in different types of instabilities. We wish to investigate these instabilities using molecular dynamics (MD) simulations.

MD simulations have provided significant insight on the behavior of membranes and in particular their prototypical model of lipid bilayers [7]. While they are appropriate in capturing the structural details of lipid bilayers, they are presently limited in their spatiotemporal resolution. The response of cell membranes to flow shear occurs in time scales that are beyond the simulation capabilities of MD. Here, we

resort to coarse-grained molecular dynamics (CGMD) [8–10] that extend the spatiotemporal resolution of MD at the expense of detailed structural descriptions, but at the same time allow us to capture microscale phenomena with detail that is beyond the capabilities of continuum simulations of membranes [11–13].

The results of the CGMD provide us with insight on the evolution of instabilities of lipid bilayers subjected to shear. We observe bucklinglike deformation in the direction perpendicular to the shear and a subsequent localized Kelvin-Helmholtz-like instability that leads to membrane rupture. The results demonstrate that the perturbation on the microscopic structure of the membrane causes such instabilities on the larger scale, indicative of both fluidlike and solidlike characteristics.

### II. COMPUTATIONAL MODEL

We study a lipid bilayer composed of dipalmitoyl phosphatidylcholine (DPPC) molecules immersed in water. The membrane and the water are modeled using the MARTINI2.0 [14] force field. In the MARTINI force field, groups of four nonhydrogen atoms are mapped into single interaction sites and one CG particle represents four water molecules. The DPPC molecule model consists of 12 CG particles [cf. Fig. 1(a)]. Two of the particles are hydrophilic: the choline and phosphate groups having positive and negative charges, respectively. The molecule is branched into two hydrophobic chains, and each of them consists of four CG particles. The remaining two particles between the hydrophilic and hydrophobic parts are the glycerol ester part. The bonds between two adjacent particles are described by the harmonic potential, and the bending angle comprised of the adjacent three particles are described by a harmonic cosine potential. Nonbonded interactions consist of Lennard-Jones and Coulomb potentials, both truncated at 1.2 nm using switching functions [15]. The parameters for the DPPC and water are de-

\*Present address: Department of Mechanical Engineering, Graduate School of Engineering, Kobe University, 1-1 Rokkodai-cho, Nada-ku, Kobe 657-8501, Japan; hanasaki@mech.kobe-u.ac.jp; hanasaki@me.es.osaka-u.ac.jp

†walther@inf.ethz.ch

‡kawano@me.es.osaka-u.ac.jp

§petros@ethz.ch

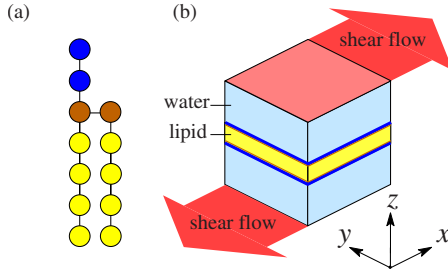


FIG. 1. (Color online) Schematic view of the computational model: (a) coarse-grained DPPC lipid molecule model [14] consisting of hydrophilic (blue: the upper two particles in dark gray), hydrophobic (yellow: the bottom eight particles in light gray), and intermediate (brown: the middle two particles in gray), and (b) configuration of the membrane and shear flow.

scribed in [14], and the details on the switching functions are described in [15].

We consider as a base configuration a lipid bilayer with a projected area of  $20 \times 20 \text{ nm}^2$  in the  $xy$  plane (cf. Fig. 1). The simulation involves 1250 DPPC molecules and 52 500 CG water particles. In addition, in order to study the different modes of membrane undulation, we consider membrane sizes of  $8 \times 20$  and  $20 \times 8 \text{ nm}^2$  consisting of 500 lipid molecules and 21 000 CG water particles. The domain size in the membrane thickness direction ( $z$ ) is determined *a posteriori* by the application of barostat [16] at 1 bar in the  $z$  direction alone. The equilibrated thicknesses of the domains are 20 nm for all of the three types of systems.

Periodic boundary conditions are applied in all directions during the equilibration procedure. The equations of motion are solved using the leap-frog algorithm with a time step of 20 fs. The temperature of the system is maintained at 323 K using a Berendsen heat bath [16]. After the equilibration, the membrane-water system is subjected to nonperiodic boundary conditions in the  $z$  direction using the boundary force algorithm proposed in Refs. [17,18].

The system is divided into 16 bins in the  $z$  direction, and the Berendsen thermostat is applied separately to each bin during the shear simulation. In order to apply the shear flow boundary condition, the adaptive body force method [19] is applied to the bins on the boundaries in the  $z$  direction of the system. Thus, imposing a velocity of  $\pm 150 \text{ nm ns}^{-1}$  across the 20 nm system results in a nominal shear rate ( $\dot{\gamma}$ ) of  $15.0 \text{ ns}^{-1}$  in the  $x$  direction.

### III. RESULTS AND DISCUSSION

We first consider the  $20 \times 20 \text{ nm}^2$  membrane subject to a shear rate of  $13.0 \text{ ns}^{-1}$  (cf. Fig. 2). The simulations display clear undulations and eventual rupture of the membrane. In the early stage, the lipid heads rotate in the direction of the shear ( $x$  direction), and the rotation and alignment result in perturbations of the membrane structure leading to a collective membrane undulation on the  $yz$  plane. A coherent large-scale deformation occurs after 10 ns. This bucklinglike undulation continues until the membrane begins to rupture at a location of large displacement and high curvature of the membrane.

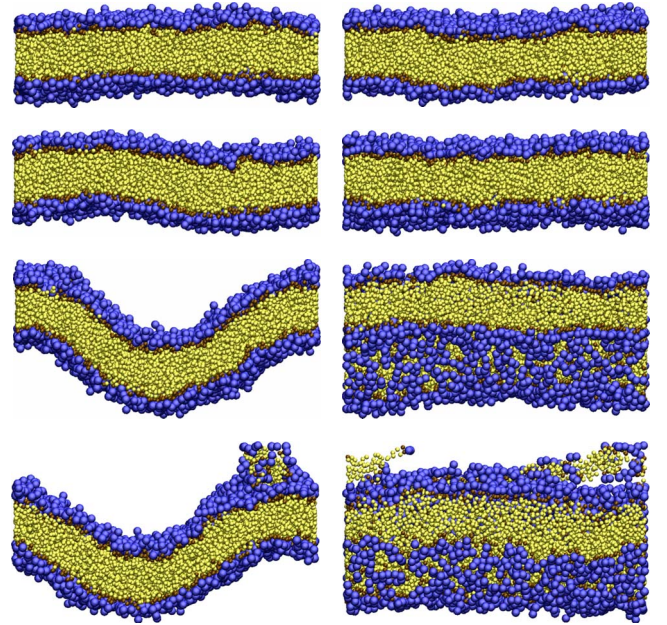


FIG. 2. (Color online) Formation of the shear-induced undulation structure and subsequent instability of the lipid membrane with domain size of  $20 \times 20 \text{ nm}^2$  at the shear rate of  $13.0 \text{ ns}^{-1}$ . Left:  $yz$  plane; right:  $xz$  plane. The 0 ns refers to the time point of turning on the shear boundary conditions. Left-hand side is the view of the  $yz$  plane and the right-hand side is that of the  $xz$  plane. The coloring (shading) of the particles corresponds to Fig. 1(a), and CG water particles are not displayed for clarity. Visual mode dynamics [20] is used for visualization of the molecules.

We observe progressively changing perturbations of the orientation of the lipid bilayer molecules when the membrane is subjected to shear. We quantify these perturbations by defining an orientation vector  $\mathbf{n} = (n_x, n_y, n_z)^T$  for the lipid molecule as the unit vector that connects the center of mass of the hydrophobic part with the center of mass of the hydrophilic part. The absolute values of the vector components are averaged, so that there is no distinction between the positive and negative directions. The value of 1 indicates that the orientation vector is aligned with the direction of the axis, and 0 indicates that it is perpendicular to it.

The temporal evolution of the averaged orientation vector components is shown in Fig. 3(a). Before imposing the shear the lipid molecules are in equilibrium, and they are largely aligned with the membrane normal direction. Once the shear is applied to the surrounding water molecules the interaction between the water and the hydrophilic part of the lipid molecules leads to an increased inclination of the lipid molecules in the direction of the shear noted by an increase in  $n_x$  and a corresponding decrease in  $n_z$ . The response time is less than 1 ns, including the time that the shear flow propagates to the membrane after turning on the shear boundary condition.  $n_y$  remains unchanged at its equilibrium for some time after  $n_x$  noticeably changes. However,  $n_y$  starts to increase at around 10 ns. The evolution of the shear components [Fig. 3(a)] indicates that the lipid molecules reorient initially in the shear direction, while the perturbation propagates on the membrane plane in the shear normal direction before any noticeable macroscale deformation of the membrane.

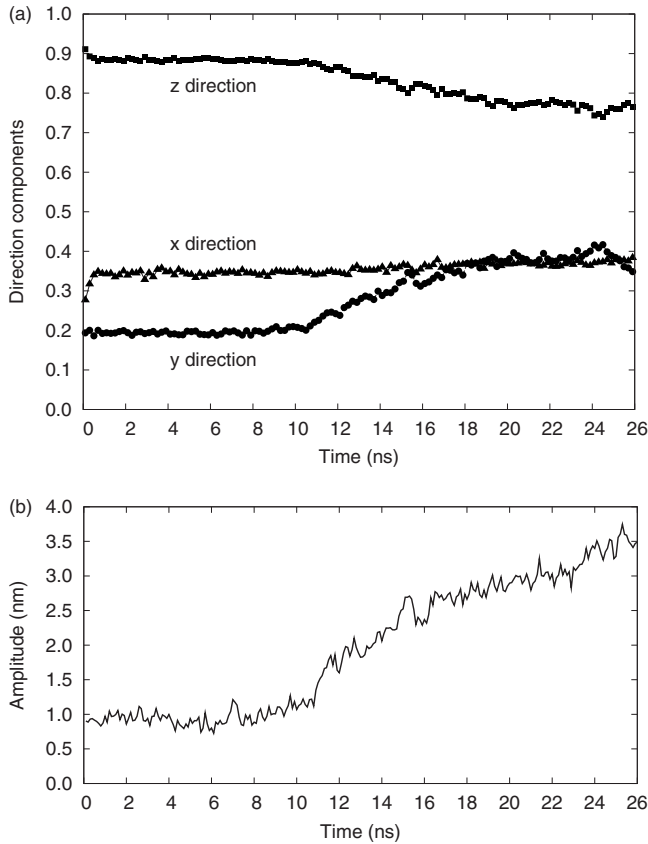


FIG. 3. Time evolution of (a) lipid molecular orientation and (b) membrane amplitude for the system with the domain size of  $20 \times 20 \text{ nm}^2$  at the shear rate of  $13.0 \text{ ns}^{-1}$ . The orientation vector  $(n_x, n_y, n_z)$  of a lipid molecule is defined by the unit vector that connects the center of mass of the hydrophobic part with the center of mass of the hydrophilic part. There is no distinction between the positive and negative directions in the molecular orientation. Denoting the maximum and minimum positions of the phosphate particles in one of the constituent layers as  $z_{\max,a}$  and  $z_{\min,a}$ , and those of the other layer as  $z_{\max,b}$  and  $z_{\min,b}$ , the amplitude  $A$  is defined as  $A = [(z_{\max,a} - z_{\min,a})/2 + (z_{\max,b} - z_{\min,b})/2]/2$ .

The continuing application of the shear eventually leads to the concerted undulation of the membrane in the  $yz$  plane. The growth of the amplitude of undulation is shown in Fig. 3(b), and it can be seen that the initiation of the amplitude growth corresponds to that of the  $n_y$  growth. There is no significant increase in the amplitude of the undulations before 10 ns, and the amplitude growth before 22 ns corresponds to the undulation structure that takes place before the rupture as shown in Fig. 2. Overall, we observe that there is no exponential growth, and the increase in the amplitude is faster at the beginning (11–16 ns) compared to the later stage (16–21 ns). The amplitude growth stops when the magnitude of  $n_y$  is equal to that of  $n_x$ , and a wavelike structure emerges in the  $y$  direction normal to the imposed shear flow.

The observed shear-induced instability of the lipid membrane in water has two components: the spanwise undulating structure with bucklinglike transition that deforms the surface normal to the direction of the shear and a Kelvin-Helmholtz-like instability parallel to the shear. These two types of instabilities are indications of the solidlike and liq-

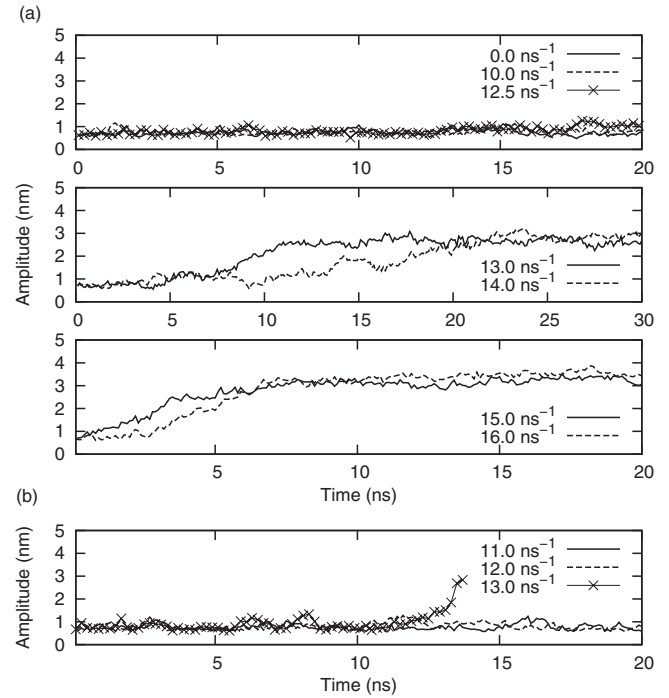


FIG. 4. Time evolution of the undulation amplitude at different shear rates for systems with domain sizes of (a)  $8 \times 20 \text{ nm}^2$  and (b)  $20 \times 8 \text{ nm}^2$ . The case of  $20 \times 8 \text{ nm}^2$  system at  $13.0 \text{ ns}^{-1}$  is plotted until the time point of rupture as shown in Fig. 6.

uidlike nature of lipid bilayers. We note here a similarity of the membrane behavior with the behavior of granular media that undergo Kelvin-Helmholtz-like instabilities [21,22]. Also similar undulations in the direction normal to the applied shear have been observed in liquid crystals [23] and more recently to multilamellar vesicles [24]. Smectic liquid crystals are multilayered structures, while the membrane is composed of a single lipid bilayer. It appears that the layering of the soft matter is not a defining factor on the orientation of undulations, leading us to investigating factors such as the relative dimensions of the membrane.

We study two additional configurations with nonequidistant  $x$  and  $y$  dimensions while maintaining the shear in the  $x$  direction. The configuration with the small  $y$  dimension ( $20 \times 8 \text{ nm}^2$ ) is used in order to reduce the bucklinglike undulations and to investigate whether a Kelvin-Helmholtz-like instability characteristic of fluid structures still occurs, while the configuration with the small  $x$  dimension ( $8 \times 20 \text{ nm}^2$ ) is used to eliminate the emergence of this fluidlike instability.

When we impose shear onto the  $8 \times 20 \text{ nm}^2$  system the membrane is undulating, yet it is stable at the shear rate of  $15.0 \text{ ns}^{-1}$ . We note that for the same shear rate the nominal configuration of  $20 \times 20 \text{ nm}^2$  ruptured at around 5 ns (not shown). Figure 4(a) shows the time evolution of the undulation amplitude as a function of time. We observe that the amplitude converges to the finite value within 10 ns. The snapshot of such undulation structure is shown in Fig. 5. Since the mesoscopic change of state in the  $x$  direction is effectively suppressed by the small domain length in that direction, the undulation structure can be clearly observed. We observed the rupture of the membrane at the higher shear

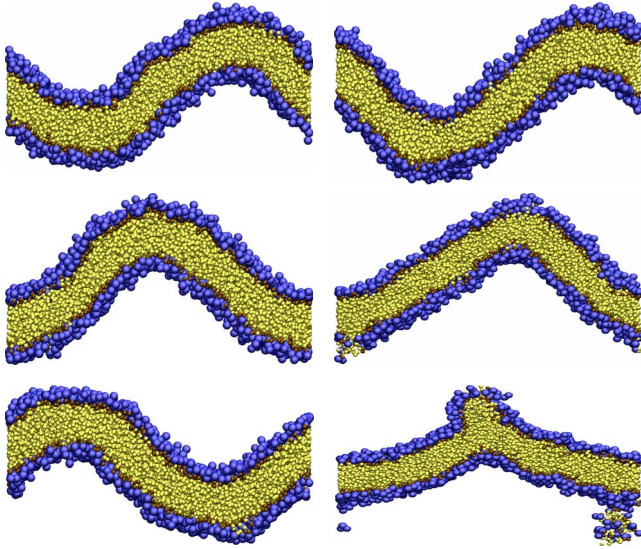


FIG. 5. (Color online) Shear-induced undulation structure with domain size of  $8 \times 20 \text{ nm}^2$  at shear rates of  $15.0 \text{ ns}^{-1}$  (left) and  $17.5 \text{ ns}^{-1}$  (right). The view is in the  $yz$  plane.

rate of  $17.5 \text{ ns}^{-1}$ , while no rupture was observed for a simulation of  $20 \text{ ns}$  at a shear rate of  $16.0 \text{ ns}^{-1}$ . Notably the location of the onset of rupture is the same as in the case of  $20 \times 20 \text{ nm}^2$ . It can also be observed that the rupture is qualitatively similar to the plastic buckling of a solid membrane or beam where the strain is finally localized. The localization of the strain that leads to folding has been observed for the thin elastic membrane located on a fluid interface [25]. Such transition is caused by an in-plane compression.

As shown in Fig. 4(a), it is found that the spanwise undulation structures of the ( $8 \times 20 \text{ nm}^2$ ) system start growing immediately after imposing the shear boundary condition, and it maintains a constant magnitude for the case of high shear rates such as  $15.0$  and  $16.0 \text{ ns}^{-1}$ . The complete structure is preserved throughout the simulation. When the simulation domain is defined such that the membrane has the reference size of  $20 \times 8 \text{ nm}^2$ , the undulation structure in the spanwise, i.e.,  $y$ , direction is suppressed. The shear flow induces perturbation on the membrane structure that changes with time as shown in Fig. 6. When the shear rate is sufficiently high, such perturbation can lead to the instability of the membrane structure. The instability is similar to a Kelvin-Helmholtz instability as shown in Fig. 6. The nonlinear wave (Fig. 6 at  $13.5 \text{ ns}^{-1}$ ) grows into a sigmoidal shape (Fig. 6 at  $13.8 \text{ ns}^{-1}$ ) before rupture. However, the nature of the amplitude growth is different. Figure 4(b) shows that the amplitude remains close to the equilibrium value at  $12.0 \text{ ns}^{-1}$  for the  $20 \times 8 \text{ nm}^2$  system. At  $13.0 \text{ ns}^{-1}$ , it is indistinguishable for some period of time with the case of  $12.0 \text{ ns}^{-1}$ , but then experiences an abrupt increase in amplitude corresponding to a Kelvin-Helmholtz-like instability (cf. Fig. 6). The growth of the Kelvin-Helmholtz-like instability is substantially faster than that of the spanwise undulation structure.

Kelvin-Helmholtz instability generally occurs when a material is subject to shear or when there is a sufficient velocity

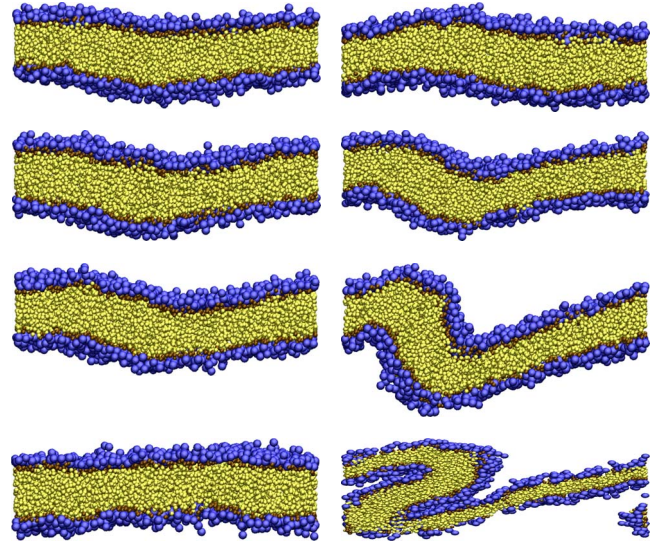


FIG. 6. (Color online) Kelvin-Helmholtz-like instability observed in the system with domain size of  $20 \times 8 \text{ nm}^2$  at shear rates of  $12.0 \text{ ns}^{-1}$  (left) and  $13.0 \text{ ns}^{-1}$  (right). The view is in the  $xz$  plane.

difference across the interface of the material. We have investigated the amount of bilayer slip in the present study and find that the lipid layers do display a finite slip. Hence, the  $20 \times 20 \text{ nm}^2$  system subject to a shear rate of  $13 \text{ ns}^{-1}$  exhibits a slip of  $11 \text{ m/s}$  in the flow direction; for the  $20 \times 8 \text{ nm}^2$  system we measure slip velocities of  $6.6$ ,  $4.5$ , and  $13 \text{ m/s}$  for shear rates of  $12$ ,  $13$ , and  $15 \text{ ns}^{-1}$ , respectively. The  $8 \times 20 \text{ nm}^2$  system appears to have a constant slip of approximately  $5 \text{ m/s}$  for all the imposed shear rates. Thus, while we do observe a slip the magnitude of the slip does not appear to correlate with the instability. Hence, we conclude that the Kelvin-Helmholtz-like instability is caused by the fluid shear.

Figure 7 shows the shear rate dependence of molecular orientation and undulation amplitude for the systems with reference membrane sizes of  $8 \times 20$  and  $20 \times 8 \text{ nm}^2$ . Figure 7(a) shows that the direction vector component  $n_x$  increases smoothly with increasing shear rate. On the other hand,  $n_y$  does not change noticeably up to the shear rate of  $12.5 \text{ ns}^{-1}$ , and there is a jump at  $13.0 \text{ ns}^{-1}$ . This jump corresponds to the threshold of stability between flat shape and undulation structure, which is shown as the amplitude in Fig. 7(b).

The sharp increase in the amplitude undulation between  $12.5$  and  $13.0 \text{ ns}^{-1}$  in Fig. 7(b) is attributed to the fact that the membrane thickness  $4 \text{ nm}$  is not negligible compared to the domain length of  $20 \text{ nm}$ . This is analogous to well-known Euler buckling phenomena [26] observed in solids. We note however that here the constituent molecules of the lipid membrane have fluid characteristics, and the instability is triggered by the transition of the microscopic state as detailed above. The undulation amplitude increases with increasing shear rate after the transition.  $n_x$  increases smoothly from the vicinity of the equilibrium state up to the shear rate that leads to rupture. The trend of molecular orientation for the system of  $20 \times 8 \text{ nm}^2$  agrees well to the case of  $8 \times 20 \text{ nm}^2$  up to  $12.0 \text{ ns}^{-1}$ , which is close to the threshold

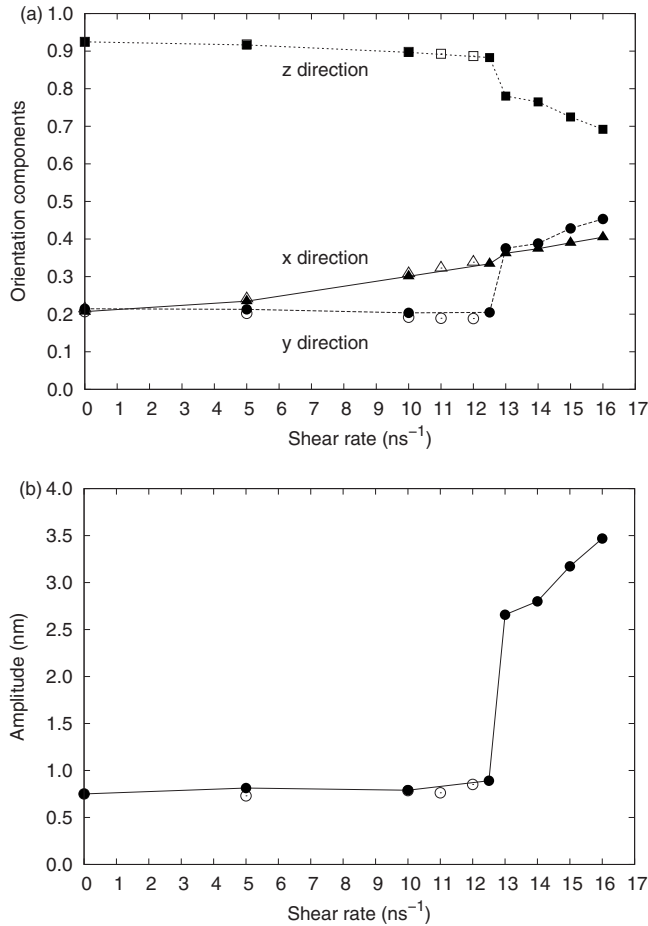


FIG. 7. Shear rate dependence of (a) molecular orientation and (b) undulation amplitude for systems with domain sizes of  $8 \times 20 \text{ nm}^2$  (filled symbols with lines) and  $20 \times 8 \text{ nm}^2$  (open symbols). The values under each shear rate is calculated by the time average from 10.0 to 20.0 ns (except for 13.0 and 14.0 ns<sup>-1</sup> by 20.0–30.0 ns) with an interval of 0.1 ns after turning on the shear boundary condition.

value. In fact, the transition point for spanwise undulation of the  $8 \times 20 \text{ nm}^2$  system and that for the Kelvin-Helmholtz-like instability of  $20 \times 8 \text{ nm}^2$  is the same within the resolution of our data.

In summary we observe two possible routes for instability at the same flow shear rate. When the size of the membrane is not constrained the Kelvin-Helmholtz-like instability is avoided at the first stage by the spanwise buckling beyond the transition point. However, the wavy membrane structure finally ruptures as the undulation structure is not sufficient to maintain the membrane structure under the shear flow or to accommodate the nonequilibrium molecular orientation. The observed instability phenomenon is somewhat different from the case of  $20 \times 8 \text{ nm}^2$  in that the  $20 \times 20 \text{ nm}^2$  system is fully three dimensional. The Kelvin-Helmholtz-like wave in the shear ( $x$ ) direction does not grow uniformly throughout

the  $y$  direction. The part of the highest curvature is mechanically less stable than the rest of the membrane, and the vicinity of the part of highest amplitude is subject to the highest shear velocity of the surrounding fluid. Therefore, the instability initiates there and not uniformly throughout the domain.

In order to examine the extent of the analogy between the observed phenomena and the Euler's buckling, we have also conducted simulations with a longer domain size in the  $y$  direction, i.e.,  $8 \times 40 \text{ nm}^2$  to compare with  $8 \times 20 \text{ nm}^2$ . The critical shear rate for the 40-nm-long domain is  $7 \text{ ns}^{-1}$ , whereas the instability occurs at  $13 \text{ ns}^{-1}$  for the 20-nm-long domain (Fig. 7). Hence, the critical shear rate decreases with increasing domain size, and the wavelength is equal to the domain size as shown in Fig. 5. This is similar to the properties of macroscopic beam structure with the assumption that the shear flow causes the compressed state of the membrane in the  $xy$  plane. The observed dependence of the critical shear rate on the domain size  $L$  (in the direction of compression) is not the  $L^2$  scaling expected for Euler buckling, but rather  $L$  scaling. This is partly attributed to the fact that the phenomena observed here involves the different elementary process that the compressed state is caused by the transition of molecular orientation as discussed above. The absolute value of the physical parameters that triggers the instability can vary depending on the domain size. The quantification of this value is however beyond the scope of the present work. The instability may be initiated by the first mode of buckling or be associated with a characteristic wavelength independent of the domain size.

There are experimental studies of membrane subject to shear flow (e.g., [27–29]), but the elementary process is not measured in these studies. What we can confirm at the present state is that Tanzeglock *et al.* [27] observed the critical shear stress corresponding to approximately  $1500 \text{ s}^{-1}$  when exposed to a laminar flow through the macroscopic membrane. This agrees with our result that the larger membrane size leads to lower critical shear rates.

#### IV. CONCLUDING REMARKS

The present study of the effects of shear flow over lipid bilayer membranes has demonstrated a dual solid-fluid response of the lipid bilayer that depends on the flow shear rate. The shear induces at first an inclination of the lipid molecules in the direction of the shear. As the shear rate is increased this deformation results in a bucklinglike instability along the spanwise direction and a subsequent Kelvin-Helmholtz instability that leads to rupture.

The present mesoscale simulations provide insight into the instabilities induced by the shear flow. We find that the perturbation on the molecular level leads to the instabilities characteristic of both fluid and solid behaviors on the continuum level.

- [1] A. Y. Fu, C. Spence, A. Scherer, F. H. Arnold, and S. R. Quake, *Nat. Biotechnol.* **17**, 1109 (1999).
- [2] J. C. Lasheras, *Annu. Rev. Fluid Mech.* **39**, 293 (2007).
- [3] J. Folkman, *Annu. Rev. Med.* **57**, 1 (2006).
- [4] J. M. Rutkowski and M. A. Swartz, *Trends Cell Biol.* **17**, 44 (2007).
- [5] J. de Jong, R. G. H. Lammertink, and M. Wessling, *Lab Chip* **6**, 1125 (2006).
- [6] D. M. Hallow, R. A. Seeger, P. P. Kamaev, G. R. Prado, M. C. LaPlaca, and M. R. Prausnitz, *Biotechnol. Bioeng.* **99**, 846 (2008).
- [7] T. Schlick, R. D. Skeel, A. T. Brunger, L. V. Kalé, J. A. Board, Jr., J. Hermans, and K. Schulten, *J. Comput. Phys.* **151**, 9 (1999).
- [8] A. Arkhipov, P. L. Freddolino, K. Imada, K. Namba, and K. Schulten, *Biophys. J.* **91**, 4589 (2006).
- [9] S. J. Marrink, A. H. de Vries, and A. E. Mark, *J. Phys. Chem. B* **108**, 750 (2004).
- [10] C. F. Lopez, P. B. Moore, J. C. Shelley, M. Y. Shelley, and M. L. Klein, *Comput. Phys. Commun.* **147**, 1 (2002).
- [11] U. Seifert, *Adv. Phys.* **46**, 13 (1997).
- [12] R. Jahn and H. Grubmüller, *Curr. Opin. Cell Biol.* **14**, 488 (2002).
- [13] Y. Kozlovsky and M. M. Kozlov, *Biophys. J.* **82**, 882 (2002).
- [14] S. J. Marrink, H. J. Risselada, S. Yefimov, D. P. Tieleman, and A. H. de Vries, *J. Phys. Chem. B* **111**, 7812 (2007).
- [15] R. Baron, D. Trzesniak, A. H. de Vries, A. Elsener, S. J. Marrink, and W. F. van Gunsteren, *ChemPhysChem* **8**, 452 (2007).
- [16] H. J. C. Berendsen, J. P. M. Postma, W. F. van Gunsteren, A. DiNola, and J. R. Haak, *J. Chem. Phys.* **81**, 3684 (1984).
- [17] E. M. Kotsalis, J. H. Walther, E. Kaxiras, and P. Koumoutsakos, *Phys. Rev. E* **79**, 045701(R) (2009).
- [18] E. M. Kotsalis, I. Hanasaki, J. H. Walther, and P. Koumoutsakos, *Comput. Math. Appl.* **59**, 2370 (2010).
- [19] J. H. Walther, T. Werder, R. L. Jaffe, and P. Koumoutsakos, *Phys. Rev. E* **69**, 062201 (2004).
- [20] W. Humphrey, A. Dalke, and K. Schulten, *J. Mol. Graphics* **14**, 33 (1996).
- [21] D. J. Goldfarb, B. J. Glasser, and T. Shinbrot, *Nature (London)* **415**, 302 (2002).
- [22] M. P. Ciamarra, A. Coniglio, and M. Nicodemi, *Phys. Rev. Lett.* **94**, 188001 (2005).
- [23] T. Soddemann, G. K. Auernhammer, H. Guo, B. Dünweg, and K. Kremer, *Eur. Phys. J. E* **13**, 141 (2004).
- [24] S. Koschoreck, S. Fujii, P. Lindner, and W. Richtering, *Rheol. Acta* **48**, 231 (2009).
- [25] L. Pociavsek, R. Dellsy, A. Kern, S. Johnson, B. Lin, K. Y. C. Lee, and E. Cerda, *Science* **320**, 912 (2008).
- [26] R. M. Jones, *Buckling of Bars, Plates, and Shells* (Bull Ridge Publishing, Blackburg, VA, 2006).
- [27] T. Tanzeglock, M. Soos, G. Stephanopoulos, and M. Morbidelli, *Biotechnol. Bioeng.* **104**, 360 (2009).
- [28] P. Jönsson, J. P. Beech, J. O. Tegenfeldt, and F. Höök, *Langmuir* **25**, 6279 (2009).
- [29] V. Kantsler, E. Segre, and V. Steinberg, *Phys. Rev. Lett.* **99**, 178102 (2007).